Optimizing the storage and retrieval efficiency of a solid-state quantum memory through tailored state preparation

Matthew D. Eisaman[a], Sergey Polyakov[a,b], Michael Hohensee[c], Jingyun Fan[a,b], Philip Hemmer[d], and Alan Migdall[a,b]

[a]Optical Technology Division, National Institute of Standards and Technology, 100 Bureau Drive, Mail Stop 8441, Gaithersburg, MD 20899-8441, USA;
[b]Joint Quantum Institute, National Institute of Standards and Technology, and University of Maryland, Department of Physics, University of Maryland, College Park, MD 20742, USA;
[c]Physics Department, Harvard University, 17 Oxford St., Cambridge, MA 02138, USA;
[d]Department of Electrical and Computer Engineering, Texas A&M University, 214 Zachry Engineering Center, College Station, Texas 77843-3128, USA

ABSTRACT

We theoretically investigate the feasibility of using spectral hole burning in Pr^{3+}:Y_2SiO_5 to prepare an ensemble of Pr^{3+} ions with a spectral distribution optimized for use as a quantum memory for single-photon states. We introduce figures of merit for the spectral distribution of the Pr^{3+} ions when used as a quantum-memory node in a Duan-Lukin-Cirac-Zoller-type quantum-repeater scheme. Finally, we describe progress toward optimizing the hole-burning sequence by using a computational model of the hole-burning process to calculate these figures of merit over a wide range of parameters.

Keywords: quantum memory, quantum repeater, rare-earth ion-doped crystal

1. INTRODUCTION

All realistic schemes for quantum communication are currently based on the use of photonic channels. However, long-distance communication is hampered by the optical loss that increases exponentially with distance, drastically reducing the communication rate. Quantum repeaters, first introduced in 1998,[1] can overcome the exponential increase of optical loss with distance by dividing the communication channel into many segments, generating and purifying entanglement for each section individually, and then extending this entanglement over longer distances via entanglement swapping. Due to the probabilistic nature of purification protocols, efficient implementation of a quantum repeater requires quantum memory. The requirement of quantum memory suggests that we need to store the local qubits in matter-based internal states instead of photonic states, because it is difficult to store photons for long times.

Rare-earth ion-doped crystals are promising candidates for use as a quantum memory for photon states due to the long ground-state coherence times of the ionic ensembles. Recent experiments using Pr^{3+}-doped Y_2SiO_5 (Pr^{3+}:Y_2SiO_5) have demonstrated decoherence times of tens of seconds,[2,3] and storage and retrieval of classical optical pulses using electromagnetically induced transparency (EIT) with storage times up to 10 s.[4] These times are 4 orders of magnitude longer than EIT storage times demonstrated for classical optical pulses in atomic gases,[5,6] and 6 orders of magnitude longer than the quantum state storage times demonstrated thus far in atomic gases.[7–9]

Due to the large inhomogeneous broadening in rare-earth ion-doped crystals (10 GHz for Pr^{3+}:Y_2SiO_5 [10]), preparation of the initial state of the ionic ensemble is required to isolate a spectral subpopulation with similar transition frequencies. State preparation in these systems is typically accomplished via spectral hole-burning techniques,[10,11] in which a spectral subpopulation of ions in a specific hyperfine ground state is isolated by first

---

Further author information: (Send correspondence to M.D.E.)
M.D.E.: E-mail: matthew.eisaman@nist.gov

optically pumping a large spectral width (5 MHz -10 MHz) of ions to other ground states (hole-burning), and then pumping back a narrow (100 kHz-1 MHz) inhomogeneously broadened spectral distribution (an anti-hole) into the desired hyperfine state.

We are interested in the practical aspects of using Pr^{3+}:Y_2SiO_5 as a quantum memory for photon states, with a special interest in optimization for use in specific quantum-repeater protocols, such as the Duan-Lukin-Cirac-Zoller (DLCZ) scheme.[12] In our contribution, we theoretically investigate the feasibility of using spectral hole burning in Pr^{3+}:Y_2SiO_5 to prepare an ensemble of Pr^{3+} ions with a spectral distribution optimized for use as a quantum memory for single-photon states. Our work considers a recent theoretical investigation into the importance of the inhomogeneously broadened spectral lineshape of an ensemble to the storage and retrieval efficiency.[13] In Sec. 1.1, we give a brief introduction to the DLCZ quantum-repeater scheme. In Sec. 1.2, we discuss the details of how Pr^{3+}:Y_2SiO_5 can be used as a quantum-memory node in the DLCZ scheme, including a discussion of the required state preparation. In Sec. 2, we describe the details of the calculation used to model the hole-burning process. Finally, in Sec. 3 we describe the results of using this model to find the optimum hole-burning sequence to produce the desired spectral distribution. Specifically, we introduce figures of merit for the spectral distribution of the Pr^{3+} ions when used as a quantum memory node in a DLCZ-type quantum-repeater scheme, and we optimize the hole-burning sequence by using a computational model of the spectral hole burning process to calculate these figures of merit over a wide range of parameters.

1.1 DLCZ Quantum-Repeater Scheme

An important conceptual step toward the realization of quantum repeaters was made in 2001, with the DLCZ proposal for long-distance quantum communication using atomic ensembles and linear optics.[12] Figure 1(a) illustrates how spontaneous photon scattering from an ensemble of atoms, combined with conditional quantum measurement, can be used to implement the backbone of this protocol - the probabilistic generation of quantum entanglement between two atomic ensembles using an absorbing photonic channel. Two atomic ensembles (represented as a three-level atom with two metastable ground states $|g\rangle$ and $|s\rangle$, and excited state $|e\rangle$) are each optically pumped into the ground state $|g\rangle$, and then illuminated by synchronized classical laser pulses (referred to as the write laser). The forward-scattered photons (referred to as Stokes photons because they are shifted to a smaller frequency) interfere at a 50% -50% beam splitter, with the outputs detected, respectively, by two single-photon detectors. The basic idea is that in such a configuration, a single detector click implies that one quantum of atomic excitation into the state $|s\rangle$ has been created in one of the two ensembles, but it is fundamentally impossible to determine which of the two ensembles emitted the photon. In this case, the measurement projects the state onto an entangled state of the two ensembles of the form

$$(1/\sqrt{2}) \cdot (|0\rangle_L |1\rangle_R + e^{i\phi} |1\rangle_L |0\rangle_R), \tag{1}$$

where L(R) labels the left (right) ensemble, $|n\rangle_i$ denotes n atomic excitations in ensemble i, and ϕ denotes an unknown phase-shift difference between the left and right channels.[12] Fig. 1(b) demonstrates how this generated entanglement, combined with the nonzero decoherence time of the $|g\rangle$ - $|s\rangle$ coherence, and the retrieval of this coherence, can be used to efficiently extend this entanglement to large distances. The entanglement between atomic ensembles created over a characteristic absorption length, L_{abs}, in the first step, indicated by filled circles connected by a line, is extended to two absorption lengths via entanglement swapping. By repeating this process, long-distance entanglement is created.[12]

Entanglement swapping is accomplished by interference of retrieved anti-Stokes photons on a beam splitter and detection as in Fig. 1(a), provided a single anti-Stokes photon has been measured. In such a probabilistic scheme, the memory, i.e., the nonzero decay time of the $|g\rangle$ - $|s\rangle$ coherence, is essential for polynomial scaling of the required time with distance, compared to exponential scaling for the case of direct entanglement generation.[12] Since the proposal of the DLCZ protocol in 2001, significant experimental progress towards its realization has been achieved in atomic gases of alkali atoms.[7, 8, 14]

One important figure of merit in the DLCZ scheme is the ratio of the quantum memory time to the time needed for a typical operation, which in the case of the DLCZ scheme is the time required to generate entanglement between two ensembles. The polynomial scaling of time with distance in the DLCZ scheme depends on the fact that successfully generated entanglement between two nodes will be preserved by the quantum memory
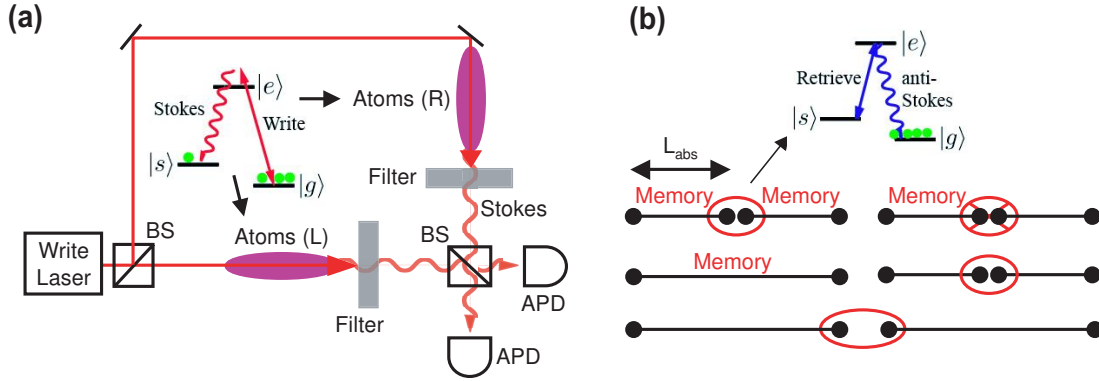
Figure 1. DLCZ quantum-repeater scheme. (a) First step: entanglement generation. Interference of spontaneous Raman-scattered Stokes photons from two ensembles (R and L) on a beam-splitter (BS) leads to generation of entanglement between the corresponding modes in the ensembles, provided a single Stokes photon was detected in one of the avalanche photo detectors (APD). If zero photons are detected, or if more than one photon is detected, the process must be repeated. (b) Second step: entanglement swapping. The entanglement between atomic ensembles created over a characteristic absorption length L_{abs} in the first step, indicated here by filled circles connected by a line, is extended to two absorption lengths via entanglement swapping. Entanglement swapping is accomplished by interference of retrieved anti-Stokes photons on a beam splitter and detection as in (a), provided a single anti-Stokes photon has been measured.

while one attempts, and sometimes fails, to generate entanglement between two other nodes. If the quantum memory decoheres before entanglement can be successfully generated between other nodes, entanglement cannot be extended via entanglement swapping, and the scaling of time with distance will no longer be polynomial. Thus far, diffusion in room-temperature atomic vapors[8] and magnetic inhomogeneities in cold atomic vapors held in magneto-optical traps,[7,14] have limited decoherence times at the single-photon level in atomic ensembles to tens of microseconds. This should be compared with the typical period of these experiments τ, divided by the probability of successful atomic excitation per repetition $p_{success}$, giving a typical operation time (i.e., entanglement-generation time) of $\tau/p_{success}$. For all experiments performed so far in atomic gases, the memory time to operation time ratio is much less than 1, whereas a ratio of much *greater* than 1 is required to achieve the polynomial scaling of time with distance enabled by the DLCZ protocol.

To overcome the decoherence-time limitations of atomic ensembles, we propose the realization of the DLCZ quantum-repeater scheme using Pr^{3+}:Y_2SiO_5 as the quantum-memory material. As previously mentioned, Pr^{3+}:Y_2SiO_5 has already been shown to have decoherence times of tens of seconds,[2,3] and was recently used to store light via EIT for up to ten seconds.[4] Even with a longer operation time, compared to alkali atoms, expected for Pr^{3+}:Y_2SiO_5 due to the longer excited-state lifetimes, a 10-second memory time would yield a memory-time-to-operation-time ratio much greater than 1.

1.2 Pr^{3+}:Y_2SiO_5 as a Quantum-Repeater Memory Node

The energy level diagram for Pr^{3+}:Y_2SiO_5 is shown in Fig. 2(a), and assumes zero magnetic field (the expected conditions for our initial experiments and the conditions for the simulations described in this paper), in which case each of the three ground and excited states are doubly degenerate. The states are conventionally labeled by the nuclear magnetic quantum numbers $\pm 1/2$, $\pm 3/2$, and $\pm 5/2$, although the nuclear wave functions are mixed due to the low site symmetry and the states are not strictly spin eigenstates.[10,11] We denote the $\pm 1/2$, $\pm 3/2$, and $\pm 5/2$ doubly-degenerate ground (excited) states as $|g, 1/2\rangle$, $|g, 3/2\rangle$, and $|g, 5/2\rangle$ ($|e, 1/2\rangle$, $|e, 3/2\rangle$, and $|e, 5/2\rangle$), respectively. Fig. 2(b) shows the pulse sequence for DLCZ entanglement-generation experiments. After preparing the ensemble of Pr^{3+} ions into a single hyperfine ground state, entanglement generation and swapping experiments are performed using the write and retrieve processes outlined in Fig. 1. As an example, Fig. 2(a) shows the $|g, 1/2\rangle$ state to be the initial state, since this is the initial state assumed in the optimization
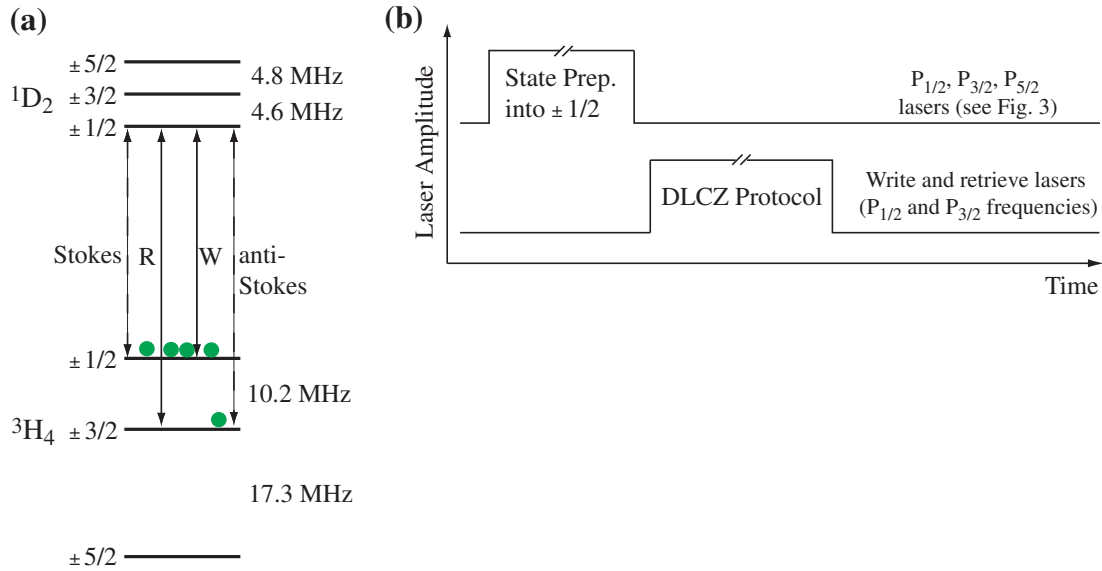
Figure 2. Specific scheme for using Pr^{3+}:Y_2SiO_5 as a DLCZ protocol quantum-memory node. (a) Energy level diagram and laser frequencies: W = write laser and R = retrieve laser. The write laser creates spontaneous Raman-scattered anti-Stokes photons, while the retrieve process retrieves the ground-state coherence onto a Stokes photon. (b) Timing sequence.

calculations performed in Sec. 3, but in principle any of the ground states could be used as the initial state *.

To use Pr^{3+}:Y_2SiO_5 as a DLCZ quantum memory node, one must not only prepare the ions in the proper initial hyperfine ground state, but also prepare the proper spectral distribution of ions. The spatially varying crystal strain throughout the Pr^{3+}:Y_2SiO_5 ensemble creates optical transition frequencies that vary from ion to ion throughout the ensemble. This leads to a broadening of the width of the optical transitions for the ensemble that is referred to as inhomogeneous broadening. The typical magnitude of inhomogeneous broadening in Pr^{3+}:Y_2SiO_5 is 10 GHz,[10] much larger than even the largest splitting (36.9 MHz = 10.2 MHz + 17.3 MHz + 4.6 MHz + 4.8 MHz) between different optical transitions for any single Pr^{3+} ion. Looking at the Pr^{3+}:Y_2SiO_5 energy-level diagram in Fig. 3(a), this means that if we apply a laser that is resonant with the $|g, 1/2\rangle - |e, 1/2\rangle$ transition for ions with zero transition-frequency shift, this laser will also be resonant with the $|g, 3/2\rangle - |e, 1/2\rangle$ transition for ions with a shift of -10.2 MHz, with the $|g, 3/2\rangle - |e, 3/2\rangle$ transition for ions with a shift of -14.8 MHz $(= -10.2$ MHz $- 4.6$ MHz$)$, and so on. However, use of Pr^{3+}:Y_2SiO_5 as a memory node in the DLCZ scheme requires the scattering and detection of a single photon from a specific hyperfine ground state (see Fig. 1). This will be impossible if in addition to the desired scattering from the $|g, 1/2\rangle$ state for ions with zero frequency shift, we also produce spontaneous Raman scattering from non-zero frequency shift ions in the other ground states. To solve this problem, we need to first prepare an initial state of the Pr^{3+}:Y_2SiO_5 ensemble in which an isolated spectral subpopulation of ions is placed in the desired hyperfine ground state, and in which the spectral distribution of all ions has been manipulated to prevent any undesired scattering from the various lasers used in the DLCZ protocol.

In the simulations described in Sec. 3, the procedure we use to prepare this initial state follows the spectral hole-burning experiments described by Nilsson et al.,[10, 11] and consists of three steps that are shown in Fig. 3. The first step uses three pump lasers (see Fig. 3.(a) and the first panel of Fig. 3(b)), and tunes the frequency of each laser to be resonant with a ground to excited state transition for each of the three ground states. In our

---

*The roles of the Stokes and anti-Stokes in Fig. 2 are opposite from the case shown in Fig. 1, but this is unimportant as it is only due to the different relative position of the two ground states in Figs. 1 and 2. The Stokes (anti-Stokes) label is only used to signify that the photon is shifted to a smaller (larger) frequency relative to the pump laser.
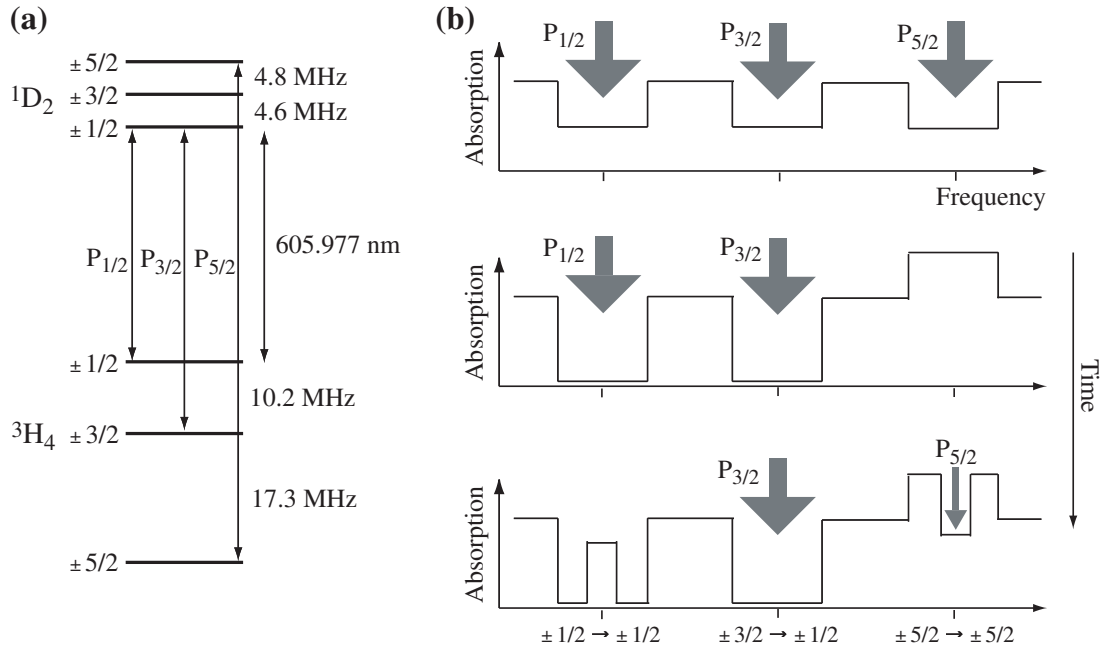
Figure 3. Procedure for preparing a spectrally narrow ensemble into the single hyperfine ground state $|g, 1/2\rangle$. (a) Level scheme showing the required laser frequencies: $P_{1/2}$ resonant with the $|g, 1/2\rangle \rightarrow |e, 1/2\rangle$ transition, $P_{3/2}$ resonant with the $|g, 3/2\rangle \rightarrow |e, 1/2\rangle$ transition, and $P_{5/2}$ resonant with the $|g, 5/2\rangle \rightarrow |e, 5/2\rangle$ transition. (b) Timing sequence.

case, we tune the pump lasers $P_{1/2}$, $P_{3/2}$, and $P_{5/2}$ to be resonant with the $|g, 1/2\rangle - |e, 1/2\rangle$, $|g, 3/2\rangle - |e, 1/2\rangle$, and $|g, 5/2\rangle - |e, 5/2\rangle$ transitions, respectively. Importantly, these lasers are tuned to be resonant with these transitions for the subset of ions with a certain frequency shift (we choose the lasers to be resonant with zero-shift ions in the simulations described in Sec. 3). Ions in this spectral subpopulation will simply be pumped among the three ground states according to the oscillator strengths of the various transitions (see Table 1). However, ions not in this spectral subpopulation, but which nevertheless are resonant with one or more of the lasers $P_{1/2}$, $P_{3/2}$, and $P_{5/2}$, will be pumped into ground states that are not resonant with any of the pump lasers. As an example, consider the case where the pump lasers are resonant with the aforementioned transitions for the subpopulation of zero-shift ions. Zero-shift ions will simply be pumped among the three ground states, since for this spectral subpopulation, each of the three ground states is resonant with one of the lasers. Ions in the -10.2 MHz-shifted subpopulation, on the other hand, will be optically pumped into the $|g, 5/2\rangle$ state, because for -10.2 MHz-shifted ions, the $|g, 3/2\rangle - |e, 1/2\rangle$ transition is resonant with the $P_{1/2}$ laser, the $|g, 1/2\rangle - |e, 5/2\rangle$ transition is near-resonant with the $P_{1/2}$ laser, and the $|g, 3/2\rangle - |e, 5/2\rangle$ transition is near-resonant with the $P_{3/2}$ laser, but no laser is resonant with -10.2 MHz-shifted ions in the $|g, 5/2\rangle$ state. This is confirmed by looking in Figs. 5(a)-(c) at the distribution of ground-state populations for -10.2 MHz-shifted ions after step 1 of the hole-burning procedure.

After the spectral subpopulation of interest has been isolated in step 1, the second step (see the second panel of Fig. 3(b)) uses lasers $P_{1/2}$ and $P_{3/2}$ to empty from states $|g, 1/2\rangle$ and $|g, 3/2\rangle$ those ions with frequency shifts spanning from frequency ω_{hole1} to frequency ω_{hole2}, with $\Delta\omega_{hole} = |\omega_{hole1} - \omega_{hole2}|$. These ions will be pumped into state $|g, 5/2\rangle$, creating a "hole" in states $|g, 1/2\rangle$ and $|g, 3/2\rangle$ spanning from ω_{hole1} to ω_{hole2}.

The third step of the state-preparation sequence (see the third panel of Fig. 3(b)) uses the $P_{5/2}$ laser to burn back an "anti-hole" into state $|1/2\rangle$ with some inhomogeneous spectral width $\Delta\omega_{anti} = |\omega_{anti1} - \omega_{anti2}|$ spanning from frequency ω_{anti1} to frequency ω_{anti2}. During this step, the $P_{3/2}$ laser is applied to make sure the anti-hole does not populate the $|g, 3/2\rangle$ state. The $P_{5/2}$ laser is applied to the spectral subpopulation isolated in step 1, but over a narrower spectral width than the width of the holes created in step 2. This creates a spectrally narrow

anti-hole sitting inside a spectrally wider hole in the $|g, 1/2\rangle$ state, ensuring an isolated population of ions, with no scattering from ions with similar frequency shifts.

Table 1. Relative oscillator strength for transitions between $^3H_4$ and $^1D_2$ hyperfine manifolds in Pr^{3+}:Y_2SiO_5. Taken from Refs. 10 and 11. Rows (columns) correspond to transitions from different ground (excited) state hyperfine levels.

g/e	$\pm 1/2$	$\pm 3/2$	$\pm 5/2$
$\pm 1/2$	0.55	0.38	0.07
$\pm 3/2$	0.40	0.60	0.01
$\pm 5/2$	0.05	0.02	0.93

2. COMPUTATIONAL MODEL

2.1 Program Description

In order to optimize the hole-burning sequence to create a spectral distribution with the desired properties in the proper hyperfine ground state, we created a computational model of the hole-burning process. The model uses a truncated Floquet expansion of the semiclassical density matrix equations of motion for a single ion. For simple field configurations, the steady-state solution for the ionic density matrix can be obtained by transforming into a rotating frame in which the equations of motion are time-independent, setting all time-derivatives to zero, and solving the resultant matrix equation. More complicated field configurations, in particular systems in which multiple fields couple the same optical transition, generate equations which do not have a time-independent rotating frame. To address such cases, our analysis is carried out in the Fourier domain. When a rotating frame exists, the solution for the transformed variable $\omega = 0$ is identical to the steady-state solution mentioned above. When there is no rotating frame, the set of Fourier-transformed equations is infinite. Higher-order multi-photon processes generate terms that oscillate at all harmonics of the beat frequencies between pairs and sets of fields, and contribute additional broadening and light shifts to the optical coherences coupled to the applied fields. In the limit that some of these fields are weak compared to DC interactions, the solution of a finite set A of this infinite series of equations can be approximated by the solution of set A coupled to a larger but also finite set B of higher-order terms, and which approximates further higher-order terms as zero.

To form this approximation, we have written a software package using MATLAB † that generates and solves the Fourier domain equations of motion that couple to the zero-frequency components of the diagonal of the ionic density matrix up to arbitrary order in ion-field interactions. The automatic process by which the equations are generated makes it possible to consider systems with large numbers of states as easily as simpler two or three-level systems, limited by the available computational power.

2.2 Physical Parameters

The natural excited state linewidth is taken to be $1/164$ μs $= 6.10$ kHz, with an additional coherence dephasing rate of $1/152$ μs$-1/164$ μs $= 481$ Hz, using parameters listed in Ref. 10, originally from Equall et al.[15] The ground-state relaxation rate is also taken from Ref. 10 to be $1/100$ s $= 10$ mHz, as is the 10 GHz width of the inhomogeneous distribution of the optical transition frequency. The ground state coherence dephasing rate is taken to be approximately $1/500$ μs $= 2$ kHz. The coupling coefficients for optical transitions between the different hyperfine states are taken from Ref. 10, and are listed in Table 1.

3. OPTIMIZATION PROCEDURE

Following the three-step hole-burning procedure outlined by Nilsson et al.[10,11] and described in Sec. 1.2, we optimize each of the three steps over a chosen set of pulse-sequence parameters. The optimization of each of the

---

†Certain trade names and company products are mentioned in the text or identified in an illustration in order to specify adequately the experimental procedure and equipment used. In no case does such identification imply recommendation or endorsement by the National Institute of Standards and Technology, nor does it imply that the products are necessarily the best available for the purpose.

three steps is done sequentially, with step 1 first optimized over the chosen parameter space. The state resulting from the optimization of the first step is used as input for the optimization of the second step, and so on for the third step. In the following section, we present the optimization results for step 1 over two parameters. The optimization of steps 2 and 3 will be described in a future work.

To gain a physical understanding of the system, we perform a line minimization,[16] in which we vary one parameter at a time, and then iterate until converging on a minimum. That is, we choose a starting set of parameters, and calculate the first step of the hole-burning sequence while varying one of the parameters, say parameter 1. We then set parameter 1 to the value found to minimize the figure of merit for step 1, and calculate step 1 while varying parameter 2. We set parameter 2 to its optimum value and then optimize parameter 3, until we have optimized the entire parameter space. This procedure is iterated until the difference between successive optima of a given parameter are less than some threshold value. It should be noted that the line minimization technique is not the fastest technique or the most likely to find a true global minimum, but we use it to gain a physical understanding of the system. We intend to confirm the line minimization results in future work by using a more robust technique such as the simplex method[16, 17] or simulated annealing.[16]

3.1 State Preparation, Step I: Isolating a Spectral Subpopulation

In order to find the optimum set of parameters, it is important to choose appropriate figures of merit for each step of the optimization. As discussed in Sec. 1.2, the first step involves the simultaneous application of three laser fields: one resonant with the $|g, 1/2\rangle - |e, 1/2\rangle$ transition ($P_{1/2}$), one resonant with the $|g, 3/2\rangle - |e, 1/2\rangle$ transition ($P_{3/2}$), and one resonant with the $|g, 5/2\rangle - |e, 5/2\rangle$ transition ($P_{5/2}$). It is important to note that "resonant" here means resonant for that spectral subpopulation of ions with zero frequency shift. The important point is that there is one laser resonant with each of the ground states; the specific excited states are chosen for their oscillator strengths to the various excited states (see Table 1). As mentioned earlier, the goal of this first step is to optically pump all ions with nonzero frequency shift to ground states that are not coupled to any excited state by the three laser fields resonant with the zero-shift atoms. This ensures that in the remaining state preparation, these laser frequencies will only interact with a spectral subpopulation of ions with zero frequency shift.

The details of the pulse sequence we use for step 1 follow the appendix of Ref. 10. We want to define a spectral subpopulation of some spectral width $\Delta\omega_{pop} = |\omega_{pop1} - \omega_{pop2}|$ spanning from a start frequency shift ω_{pop1} to a stop frequency shift ω_{pop2} by sweeping the frequency of the pump lasers $P_{1/2}$, $P_{3/2}$, $P_{5/2}$. The Rabi frequencies of these lasers are defined as $\Omega_{1/2}$, $\Omega_{3/2}$, and $\Omega_{5/2}$, respectively. We simultaneously sweep the frequencies of all three pump lasers in a time t_{sweep}, so that each laser is resonant with ω_{pop1}-shifted ions at the start of the sweep, and ω_{pop2}-shifted ions at the end of the sweep. The lasers are not on continuously, but rather pulsed on and off. The total sweep time t_{sweep} is subdivided into periods of duration $t_{rep} = 1/\nu_{rep}$, where ν_{rep} is the pulse repetition rate. Within a single t_{rep}, the lasers are all three on for a duration t_{on} at the beginning of t_{rep}; for the remainder of t_{rep}, the lasers are off for duration $t_{off} = t_{rep} - t_{on}$. The duty cycle is the percentage of time the lasers are on, and is defined as t_{on}/t_{rep}. The frequencies of all three lasers are swept simultaneously from ω_{pop1} to ω_{pop2}, with successive pulses being shifted by an amount $\omega_{step} = \Delta\omega_{pop}/(t_{sweep}/t_{rep})$. This sweep from ω_{pop1} to ω_{pop2} it repeated n_{sweep} times.

The figure of merit for the optimization of the first step should quantify the goal of isolating a subpopulation of zero-shift ions. Based on the energy-level structure for a Pr^{3+} ion with zero frequency shift shown in Fig. 2(a), for each of the three laser fields we can identify the frequency shift that would couple the field to a state other than the intended one. The figure of merit should quantify how much population is present in these undesired states at frequency shifts that will allow unwanted coupling. For the $P_{1/2}$ field, a shift of -10.2 MHz for an ion in the $|g, 3/2\rangle$ state allows resonant coupling of the $|g, 3/2\rangle - |e, 1/2\rangle$ transition, a shift of -14.8 MHz $= (-10.2$ MHz $- 4.6$ MHz$)$ allows resonant coupling of the $|g, 3/2\rangle - |e, 3/2\rangle$ transition, and a shift of -19.6 MHz $= (-10.2$ MHz $- 4.6$ MHz $- 4.8$ MHz$)$ allows resonant coupling of the $|g, 3/2\rangle - |e, 5/2\rangle$ transition. Similarly, shifts of -27.5 MHz , -32.1 MHz $= (-27.5$ MHz $- 4.6$ MHz$)$, and -36.9 MHz $= (-27.5$ MHz $- 4.6$ MHz $- 4.8$ MHz$)$ allow couplings of the $|g, 5/2\rangle - |e, 1/2\rangle$, $|g, 5/2\rangle - |e, 3/2\rangle$, and $|g, 5/2\rangle - |e, 5/2\rangle$ transitions, respectively, for ions in the $|g, 5/2\rangle$ state. Since it is really coupling of these ions to the laser that we are trying to avoid, the populations should be weighted by the relevant oscillator strengths (see Table 1). A figure of merit for step 1 of

the hole-burning procedure for the field $P_{1/2}$, which we will denote as $FOM_1(P_{1/2})$, is then the weighted sum of the ground-state populations at the frequency shifts that allow various undesired couplings, where the weighting is the oscillator strength for the transition of interest. Specifically, $FOM_1(P_{1/2})$ can be written as:

$$\begin{aligned} FOM_1(P_{1/2}) &= \frac{1}{2}[O(3/2, 1/2)P(3/2, -10.2) + O(3/2, 3/2)P(3/2, -14.8) + O(3/2, 5/2)P(3/2, -19.6) \quad (2) \\ &+ O(5/2, 1/2)P(5/2, -27.5) + O(5/2, 3/2)P(5/2, -32.1) + O(5/2, 5/2)P(5/2, -36.9)], \end{aligned}$$

where O(g,e) represents the oscillator strength between the ground state g and excited state e taken from Table 1, $P(g, \omega_{shift})$ is the population remaining in ground state g for frequency shift ω_{shift}, and the factor of 1/2 multiplying the entire expression normalizes the sum of the six O(g,e) coefficients to 1 (for the O(g,e) coefficients listed in Table 1, the sum of each *three* coefficients for a given ground state are normalized to one). Ideally this sum should be zero, indicating that there is no population with frequency shifts and in states that allow unwanted scattering. Similar figures of merit, $FOM_1(P_{3/2})$ and $FOM_1(P_{5/2})$, can be calculated for the other two laser fields, $P_{3/2}$ and $P_{5/2}$ respectively

$$\begin{aligned} FOM_1(P_{3/2}) &= \frac{1}{2}[O(1/2, 1/2)P(1/2, 10.2) + O(1/2, 3/2)P(1/2, 5.6) + O(1/2, 5/2)P(1/2, 0.8) \quad (3) \\ &+ O(5/2, 1/2)P(5/2, -17.3) + O(5/2, 3/2)P(5/2, -21.9) + O(5/2, 5/2)P(5/2, -26.7)], \\ FOM_1(P_{5/2}) &= \frac{1}{2}[O(1/2, 1/2)P(1/2, 36.9) + O(1/2, 3/2)P(1/2, 32.3) + O(1/2, 5/2)P(1/2, 27.5) \quad (4) \\ &+ O(3/2, 1/2)P(3/2, 26.7) + O(3/2, 3/2)P(3/2, 22.1) + O(3/2, 5/2)P(3/2, 17.3)]. \end{aligned}$$

Since the goal of step 1 is to prevent scattering of all three of the pump lasers from ions in frequency classes other than the one of interest, the figure of merit for step 1 of the hole-burning procedure is simply the average of the figures of merit for each laser individually:

$$FOM(\text{step1}) = \frac{1}{3}\left[FOM_1(P_{1/2}) + FOM_1(P_{3/2}) + FOM_1(P_{5/2})\right]. \quad (5)$$

3.1.1 Results

For starting values of the pulse-sequence parameters of step 1, we use the same parameters as in the appendix of Ref. 10: $\Omega_{1/2} = \Omega_{3/2} = \Omega_{5/2} = 1$ MHz, $\omega_{pop1} = -3$ MHz (0 MHz is defined as a zero frequency shift), $\omega_{pop2} = +3$ MHz, $t_{rep} = 250$ μs, $t_{on} = 50$ μs, $\omega_{step} = 0.6$ MHz, and $n_{sweep} = 30$, resulting in a total number of 300 excitation pulses for step 1. We assume an initial spectral distribution that is equally distributed from -100 MHz to $+100$ MHz, with this 200 MHz-wide frequency interval discretized into 1000 frequency classes.

We perform a line optimization[16] in the two-parameter space of duty cycle (t_{on}/t_{rep}) and Rabi frequency. Fig. 4(a) shows FOM(step 1) calculated for the starting parameters described in the previous paragraph as the duty cycle is varied. t_{on} is changed to vary the duty cycle (t_{on}/t_{rep}). $t_{rep} = 250$ μs for all points. A minimum of FOM(step 1)$_{min} = 2.5 \times 10^{-2}$ at duty cycle of 55% is obtained. Note that for the starting state prior to application of the pulse sequence, FOM(step 1) $= 1/6 \approx 0.1667$, because the population is normalized to 1 and is equally distributed over 6 ground states: $\pm 5/2$, $\pm 3/2$, and $\pm 1/2$. Ideally, after the pulse sequence we want FOM(step 1) $= 0$. Therefore, a value of FOM(step 1)$_{min} = 2.5 \times 10^{-2}$ means that 15% of the population remains in states and frequency classes that allow unwanted couplings to the pump lasers. For all calculations shown in Fig. 4, we make sure that n_{sweep} is large enough to allow FOM(step 1) to reach its asymptotic steady-state value. In addition, to calculate FOM(step 1), we first run the pulse sequence, and then wait for 100 ms to allow the relaxation of the excited-state population. FOM(step 1) is calculated from the ground-state populations after the excited state populations have relaxed back to the ground states. Typical populations remaining in the excited states after waiting 100 ms at the end of the pulse sequence are on the order of a few parts times 10^{-4}.

Sitting at the optimum value of 55% duty cycle, we vary the Rabi frequency of the pump lasers (for all calculations $\Omega_{1/2} = \Omega_{3/2} = \Omega_{5/2}$), with the result shown in Fig. 4(b). For this optimization, the ratio of the Rabi frequency Ω to the frequency step between successive pulses is kept constant at $\Omega/\omega_{step} = 1.67$. Computational limitations prevented us from finding the true minimum at $\Omega < 100$ kHz. Since Ω/ω_{step} is kept constant, as Ω
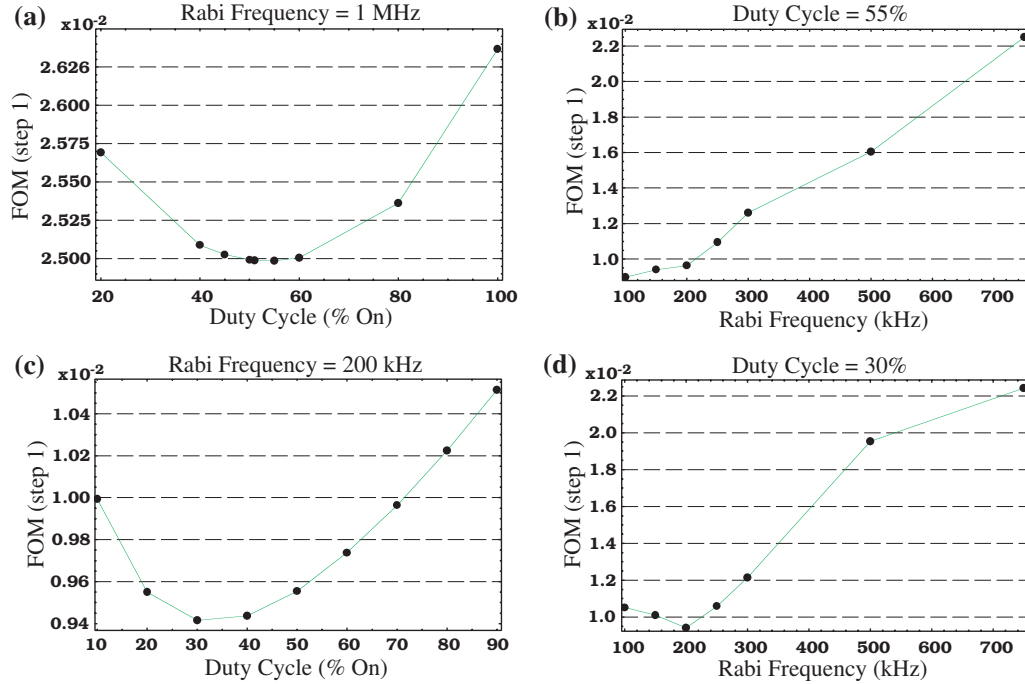
Figure 4. Optimization of step 1 over the parameter space of duty cycle and Rabi frequency Ω ($\Omega_{1/2} = \Omega_{3/2} = \Omega_{5/2} = \Omega$ in our optimization). (a) FOM (step 1) vs. duty cycle, for the starting parameter values given in the text and a Rabi frequency of 1 MHz. $t_{rep} = 250$ μs for all points; t_{on} is varied to vary the duty cycle. FOM(step 1)$_{min} = 2.5 \times 10^{-2}$ at a duty cycle of 55%. (b) FOM(step 1) as a function of Rabi frequency, for a duty cycle of 55%. $\Omega/\omega_{step} = 1.67$ for all points. Computational limitations prevented us from finding the true minimum at $\Omega < 100$ kHz. (c) FOM(step 1) as a function of duty cycle, for $\Omega = 200$ kHz. FOM(step 1)$_{min} = 0.94 \times 10^{-2}$ at duty cycle of 30%. (d) FOM(step 1) as a function of Ω, for a duty cycle of 30%. FOM(step 1)$_{min} = 0.94 \times 10^{-2}$ at $\Omega = 200$ kHz. The true minimum may be at $\Omega < 200$ kHz, since FOM(step 1) did not reach its asymptotic value for $\Omega = 150$ kHz and $\Omega = 100$ kHz.

decreases, ω_{step} decreases, thus increasing the required computational resources. In addition, the leveling off in FOM(step 1) observed for $\Omega = 150$ kHz and $\Omega = 100$ kHz is partially due to the fact that for these points, we did not have the computational resources to make n_{sweep} large enough to allow FOM(step 1) to reach its asymptotic steady-state value. Therefore, the asymptotic values of FOM(step 1) for $\Omega = 150$ kHz and $\Omega = 100$ kHz are probably slightly smaller than shown in Fig. 4(b).

In Fig. 4(c) we set the Rabi frequency to $\Omega = 200$ kHz and again vary the duty cycle. $t_{rep} = 250$ μs for all points. We chose $\Omega = 200$ kHz because it is the value of Ω with the smallest FOM(step 1) for which FOM(step 1) can achieve its asymptotic, steady-state value. We find FOM(step 1)$_{min} = 0.94 \times 10^{-2}$ at a duty cycle of 30%.

Finally, in Fig. 4(d), we set the duty cycle to 30% and vary the Rabi frequency, keeping $\Omega/\omega_{step} = 1.67$ as before. We find a minimum of FOM(step 1)$_{min} = 0.94 \times 10^{-2}$ at $\Omega = 200$ kHz. This seems to imply a convergence of the optimization, but we should caution that the true minimum in Fig. 4(d) may actually be at $\Omega < 200$ kHz, since our computational limitations prevent FOM(step 1) from reaching its asymptotic value for $\Omega = 150$ kHz and $\Omega = 100$ kHz.

Figs. 5(a)-(c) show the spectral distribution of ions in the $|g, 5/2\rangle$, $|g, 3/2\rangle$, and $|g, 1/2\rangle$ ground states, respectively, for the optimum parameters of 30% duty cycle and $\Omega = 200$ kHz. Fig. 5(d) shows a calculation of FOM$_1$(P$_{1/2}$), FOM$_1$(P$_{3/2}$), FOM$_1$(P$_{5/2}$), and FOM(step 1) as a function of time during the pulse sequence. This figure allows us to see the time-dependence of the hole-burning procedure, and to understand which subpopulation of ions in which ground states contribute most significantly to the non-zero value of FOM(step 1).
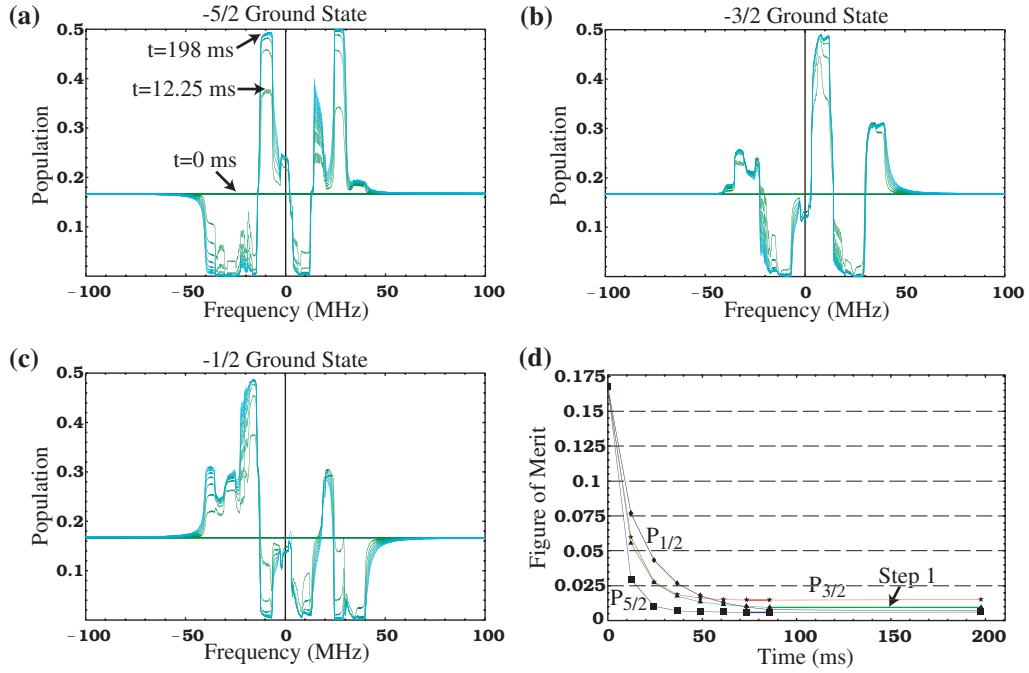
Figure 5. Spectral distribution of ions at various times during the optimum pulse sequence. For all panels, the duty cycle 30% and $\Omega = 200$ kHz. (a-c) Population of ions in the $|g, -5/2\rangle$, $|g, -3/2\rangle$, and $|g, -1/2\rangle$ states, respectively, as a function of frequency shift. (Traces for the degenerate $|g, +5/2\rangle$, $|g, +3/2\rangle$, and $|g, +1/2\rangle$ states are identical.) Nine traces are shown, for times $t = 0$, $t = 12.25$ ms, and every 12.25 ms until 85.75 ms. The last trace is at $t = 198$ ms due to the 100 ms wait after the pulse sequence to allow the excited-state population to relax. Each trace corresponds to one of the points in panel (d). (d) FOM$_1$(P$_{1/2}$), FOM$_1$(P$_{3/2}$), FOM$_1$(P$_{5/2}$), and FOM(step 1) versus time for the pulse sequence depicted in panels (a)-(c).

In future work, we would like to extend our computational capabilities to allow us to find a true minimum of Rabi frequency, and also to confirm these results with a more robust optimization method, such as the simplex method[16,17] or simulated annealing.[16] We would also like to optimize over a larger parameter space. At the time of this writing, we have not had time to perform the optimization for steps 2 and 3 of the hole-burning sequence. However, in the next two sections, we describe these steps, as well as the figures of merit that will be used in their optimization.

3.2 State Preparation, Step II: Hole Burning

In the second step of the hole-burning procedure, two laser fields are simultaneously applied: one resonant with the $|g, 1/2\rangle - |e, 1/2\rangle$ transition (P$_{1/2}$ in Fig. 3), and one resonant with the $|g, 3/2\rangle - |e, 1/2\rangle$ transition (P$_{3/2}$ in Fig. 3). The goal of this step is to empty all population of near-zero-shift ions (ions having a frequency shift in some range from ω_{hole1} to ω_{hole2}, with $\omega_{hole1} < 0 < \omega_{hole2}$) from the $|g, 1/2\rangle$ and $|g, 3/2\rangle$ states by pumping these ions to the $|g, 5/2\rangle$ state. This creates "holes" in the $|g, 1/2\rangle$ and $|g, 3/2\rangle$ state populations for ions in the frequency shift range ω_{hole1} to ω_{hole2}. The value of $\Delta\omega_{hole} = |\omega_{hole1} - \omega_{hole2}|$ should be large enough to provide a zero-population background around the anti-hole we pump back into state $|g, 1/2\rangle$ in step 3. The hole in the $|g, 3/2\rangle$ state is required to allow a zero background for the small population that is written to the $|g, 3/2\rangle$ state in the write process, and also to have zero background from which to retrieve this created coherence in the retrieve process (see Sec. 1.1).

The figure of merit for the optimization of the second step should quantify the goal of creating zero population holes in the $|g, 1/2\rangle$ and $|g, 3/2\rangle$ states over the frequency interval from ω_{hole1} to ω_{hole2}. Therefore the figure of

merit should simply be the integrated population of the $|g, 1/2\rangle$ state over the frequency range ω_{hole1} to ω_{hole2} plus the integrated population of the $|g, 3/2\rangle$ state over the frequency range ω_{hole1} to ω_{hole2}.

3.3 State Preparation, Step III: Burning Back an Anti-Hole

As shown in the third panel of Fig. 3(b), the third step involves burning back an "anti-hole" into the state $|g, 1/2\rangle$. This is accomplished by applying the $P_{3/2}$ laser to preserve the hole in the $|g, 3/2\rangle$ state created in step 2, while simultaneously applying the $P_{5/2}$ laser to pump population (referred to as an "anti-hole") into the $P_{1/2}$ state. The $P_{5/2}$ laser is applied to the zero-frequency-shift spectral subpopulation, but over a narrower spectral width than the width of the holes created in step 2. This creates a spectrally narrow anti-hole sitting inside a spectrally wider hole in the $|g, 1/2\rangle$ state, ensuring an isolated population of ions, with no scattering from ions with nearby frequency shifts.

The figure of merit we propose for step 3 is based on recent theoretical understanding of the importance of the inhomogeneously broadened spectral lineshape of an ensemble to the EIT-based storage and retrieval efficiency.[13] In the DLCZ protocol shown in Fig. 1 and described in Sec. 1.1, the write step used to generate entanglement creates an atomic coherence between hyperfine ground states that is stored in the ensemble until the retrieval step used for entanglement swapping. This retrieval step is based on EIT,[5–8] and therefore the fidelity of the quantum-memory node depends on the EIT-based retrieval efficiency. Recent work by Gorshkov et al.[13] suggests that for an inhomogeneously broadened ensemble such as the anti-hole created in step 3, the retrieval efficiency is maximized for distributions with tails that fall off faster than those of a Lorenztian distribution. We therefore propose the sharpness of the fall-off of the tails of the anti-hole spectral distribution as the figure of merit for the optimization of step 3.

4. CONCLUSIONS AND FUTURE WORK

We have described a scheme for using $Pr^{3+}:Y_2SiO_5$ as a quantum-memory node in a DLCZ-type[12] quantum repeater scheme, including a detailed description of the necessary state preparation. We have constructed a computational model of the hole-burning process used to prepare the initial spectral distribution in order to optimize the state-preparation procedure. We have introduced figures of merit for the optimization of each of the three steps of the hole-burning procedure, and found the optimum parameters for the first of these three steps. In future work, we will complete the optimization of steps 2 and 3, in addition to confirming the optimization results with a more robust optimization method such as simplex[16, 17] or simulated annealing.[16] In addition, we are constructing an experimental setup to test the optimization results, and to implement the DLCZ quantum-repeater scheme using $Pr^{3+}:Y_2SiO_5$.

ACKNOWLEDGMENTS

REFERENCES

1. H.-J. Briegel, W. Dur, J. I. Cirac, and P. Zoller, "Quantum Repeaters: The Role of Imperfect Local Operations in Quantum Communication," *Physical Review Letters* **81**, p. 5932, 1998.
2. E. Fraval, M. J. Sellars, and J. J. Longdell, "Method of Extending Hyperfine Coherence Times in $Pr^{3+}:Y_2SiO_5$," *Physical Review Letters* **92**(7), p. 077601, 2004.
3. E. Fraval, M. J. Sellars, and J. J. Longdell, "Dynamic Decoherence Control of a Solid-State Nuclear-Quadrupole Qubit," *Physical Review Letters* **95**(3), p. 030506, 2005.
4. J. J. Longdell, E. Fraval, M. J. Sellars, and N. B. Manson, "Stopped Light with Storage Times Greater than One Second Using Electromagnetically Induced Transparency in a solid," *Physical Review Letters* **95**(6), p. 063601, 2005.
5. D. F. Phillips, A. Fleischhauer, A. Mair, and R. L. Walsworth, "Storage of Light in Atomic Vapor," *Phys. Rev. Lett.* **86**, pp. 783–786, 2001.

6. C. Liu, Z. Dutton, C. H. Behroozi, and L. V. Hau, "Observation of coherent optical information storage in an atomic medium using halted light pulses," *Nature* **409**, pp. 490–493, 2001.

7. T. Chanelière, D. N. Matsukevich, S. D. Jenkins, S.-Y. Lan, T. A. B. Kennedy, and A. Kuzmich, "Storage and retrieval of single photons transmitted between remote quantum memories," *Nature* **438**, pp. 833–836, 2005.

8. M. D. Eisaman, A. André, F. Massou, M. Fleischhauer, A. Zibrov, and M. D. Lukin, "Electromagnetically induced transparency with tunable single-photon pulses," *Nature* **438**, pp. 837–841, 2005.

9. H. de Riedmatten, J. Laurat, C. W. Chou, E. Schomburg, D. Felinto, and H. J. Kimble, "Direct Measurement of Decoherence for Entanglement between a Photon and a Stored Atomic Excitation," *Physical Review Letters* **97**, p. 113603, 2006.

10. M. Nilsson, L. Rippe, S. Kroll, R. Klieber, and D. Suter, "Hole-burning techniques for isolation and study of individual hyperfine transitions in inhomogeneously broadened solids demonstrated in Pr^{3+}:Y_2SiO_5," *Physical Review B (Condensed Matter and Materials Physics)* **70**(21), p. 214116, 2004.

11. M. Nilsson, L. Rippe, S. Kroll, R. Klieber, and D. Suter, "Erratum: Hole-burning techniques for isolation and study of individual hyperfine transitions in inhomogeneously broadened solids demonstrated in Pr^{3+}:Y_2SiO_5 [Phys. Rev B **70**, 214116 (2004)]," *Physical Review B (Condensed Matter and Materials Physics)* **71**(14), p. 149902, 2005.

12. L. M. Duan, M. D. Lukin, J. I. Cirac, and P. Zoller, "Long-distance quantum communication with atomic ensembles and linear optics," *Nature* **413**, pp. 414–418, 2001.

13. A. V. Gorshkov, A. Andre, M. D. Lukin, and A. S. Sorensen, "Photon storage in lambda-type optically dense atomic media. III. Effects of inhomogeneous broadening," *http://arxiv.org/quant-ph/0612084* .

14. C. W. Chou, H. de Riedmatten, D. Felinto, S. V. Polyakov, S. J. van Enk, and H. J. Kimble, "Measurement-induced entanglement for excitation stored in remote atomic ensembles," *Nature* **438**, pp. 828–832, 2005.

15. R. W. Equall, R. L. Cone, and R. M. Macfarlane, "Homogeneous broadening and hyperfine structure of optical transitions in Pr^{3+}:Y_2SiO_5," *Phys. Rev. B* **52**(6), pp. 3963–3969, 1995.

16. W. H. Press, B. P. Flannery, S. A. Teukolsky, and W. T. Vetterling, *Numerical Recipes in C: The Art of Scientific Computing*, Cambridge University Press, New York, 1988.

17. J. A. Nelder and R. Mead, "A simplex method for function minimization," *Computer Journal* **7**, pp. 308–313, 1965.